Physica Scripta

PAPER

Experimental observation of topological phase transitions in a mechanical 1D-SSH model

RECEIVED
26 September 2021

REVISED
21 November 2021

ACCEPTED FOR PUBLICATION
25 January 2022

PUBLISHED
10 February 2022

Luke Thatcher[1], **Parker Fairfield**[1], **Lázaro Merlo-Ramírez**[2] **and Juan M Merlo**[1]

[1] Physics and Astronomy Department. Vassar College, 124 Raymond Ave. Poughkeepsie, NY, 12604, United States of America
[2] Universidad Hotelera Suiza, 23-B Sur, Puebla, 72430, Mexico

E-mail: jmerloramirez@vassar.edu

Keywords: SSH Model, topological insulators, mechanical model, band gap, edge state, phase transition

Supplementary material for this article is available online

Abstract

In this work, we report the experimental observation of the topological phase transition in a mechanical one-dimensional topological insulator using the Su-Schrieffer-Heeger (SSH) model. Our mechanical system was composed of an elastic string with metallic masses emulating atomic sites and the intra- and inter-cell interaction strengths controlled by the distances, d_1 and d_2 respectively, between the masses. We observed a trivial phase with a band gap of ~9.2 Hz $\pm$ 0.5 Hz for $d_2/d_1 = 3$, while the metallic phase closed the gap, $d_1 = d_2$, to be reopened in the topological phase as ~8.7 Hz $\pm$ 0.5 Hz, for $d_2/d_1 = 1/3$, with two edge states located inside the band gap at ~15.6 Hz $\pm$ 0.5 Hz. Our experimental observations were supported with numerical and theoretical models. Our work creates the ability to study topological phase transitions in mechanical systems with materials available in any research lab and allows an understanding of phase transitions in a visual way.

1. Introduction

Topological insulators (TIs) are a special type of material that allows electrons to occupy energy states in the band gap between the valence and conducting bands [1, 2]. These statescalled edge stateshave an exceptional ability: they are not affected by perturbations of the crystal lattice, as long as such perturbations are not magnetic [1]. The observation of the edge states in TIs in quantum systems requires the use of very sophisticated instruments and extreme conditions [3, 4]. Fortunately, it was recently demonstrated that topological phases could exist even in classical systems under the appropriate conditions [5–10]. These conditions are met when the materials are engineered to emulate the properties of quantum systems, i.e. atoms interacting in a crystal lattice by the interchange of electronic wave-functions, but with classical waves. Nowadays there are reports of topological phases in acoustic [5, 6], photonic [7, 8], and mechanical systems [9, 10]. In the case of a mechanical topological insulator, a crystal lattice can be emulated by using an array of harmonic oscillators, where the mass plays the role of an atom while the mechanical wave represents the electronic wave-function [9].

The simplest TI is composed of a one-dimensional chain of atomic sites that can support edge states [11]. It was demonstrated that polyacetylene can exhibit exotic conduction behavior due to the existence of solitons [11]. Su, Schrieffer, and Heeger proposed a model to explain the existence of solitons in polyacetylene called the SSH model that is currently a key model for the study of topology on such a structure [11]. It is important to mention that in the SSH model, there are three unique topologies that are dependent on the values of the intracell and intercell electron hopping probabilities, v and w respectively [2]. When $v > w$, the system is an insulator with a defined band gap. This is known as the trivial phase. When $v = w$, the so-called metallic phase, the system is a conductor with no band gap. Finally, when $v < w$, the system is a topological insulator and there exist edge states within the band gap. This configuration is known as the topological phase [2].

In this work, we demonstrate the existence of topological edge states in a mechanical one-dimensional SSH (1D-SSH) model composed of an elastic string with attached masses that emulate atomic sites. We confirm the existence of edge states localized at the extremes of the device. In addition, we use numerical simulations and a

© 2022 IOP Publishing Ltd

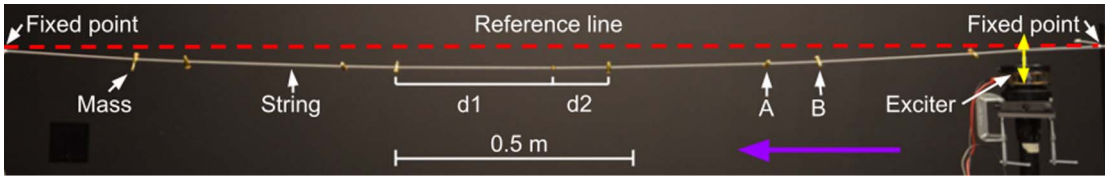

Figure 1. Experimental realization of the mechanical 1D-SSH model using an elastic string. A and B represent the positions of the emulated atomic masses. The yellow double-headed arrow indicates the direction of excitation, and the purple arrow in the bottom right indicates the direction of wave propagation. The present configuration corresponds to the topological II case.

Table 1. Values of d_1 and d_2 corresponding to the trivial, metallic, and topological cases.

d_1 (m)	d_2 (m)	d_2/d_1	Configuration
0.112	0.338	3	Trivial II
0.150	0.300	2	Trivial I
0.225	0.225	1	Metallic
0.300	0.150	1/2	Topological I
0.338	0.112	1/3	Topological II

theoretical model to confirm that our experimental observations are correctly addressed. Our mechanical model allows for easy construction and easy observation of topological edge states in a classical system. Additionally, our model can change configurations between trivial, metallic, and topological phases using one device by making only slight modifications to the system. This model allows quantum wave functions to be studied visually with a classical system.

2. Methods

2.1. Experimental methods

We implemented the mechanical version of the 1D-SSH model by using an elastic string and metallic pieces as masses. Figure 1 shows a picture of the device, where A and B refer to the atomic sites represented in the SSH model [11, 12]. We considered A and B together to be a cell, so the distance d_1 from A to B (moving right to left in the direction of wave propagation) was the intracell distance, and the distance d_2 from B to A was the intercell distance. The distances d_1 and d_2 were proportional to $1/v$ and $1/w$ in the SSH model, respectively. We therefore described our configurations using the ratio d_2/d_1, which was proportional to the ratio v/w in the SSH model. In this configuration, we expected to observe the trivial phase when $d_2/d_1 > 1$, the metallic phase when $d_2/d_1 = 1$, and the topological phase for $d_2/d_1 < 1$.

We excited the first B site on the right side of the setup using a mechanical vibrator, exciter in figure 1, controlled by a function generator. We used a square wave function at amplitude voltages between 6.0 V and 10.0 V. We swept through frequencies and determined the resonant frequencies (modes) of the string by identifying frequencies that corresponded to the maximum amplitude of oscillation for each normal mode [13].

In order to modify the configurations between trivial, metallic, and topological phases, we kept the B sites in place and moved the A sites to change the values of the distances d_1 and d_2, see figure 1. The simplicity of this setup allowed us to position the A sites anywhere in a continuum between the B sites. We could therefore achieve any value of d_2/d_1, up to the uncertainty of our measurements of each site's position. However, as we were interested in demonstrating the topological edge modes in our device, we only used two values of d_2/d_1 for the trivial and topological phases. The corresponding configurations for the values of d_1 and d_2 are shown in table 1. Note that these values were chosen for simplicity of the ratio d_2/d_1, though any other set of values could have generated the same results.

We used a stroboscopic lamp flashing at the excitation frequency to identify the normal modes of our system and took pictures of each mode using a camera in a fixed position. We used an exposure time of 1 second to capture multiple periods of oscillation of each identified mode.

In order to measure the oscillation amplitudes of the metallic masses at the edge states of the topological II configuration, we used a tracking software and called y the vertical displacement of each A site. Next, we

calculated the energy of each site as: $E = \frac{1}{2}k_A y^2$, where $k_A = 75.0 \pm 2.9$ N m^{-1} was the transverse elasticity constant. This will be discussed in further detail in the Results section.

2.2. Numerical methods

In order to support our experimental results, we used a numerical model that emulated the conditions of our experiment. We used COMSOL MULTIPHYSICS for the numerical modeling of our system. The material properties of the elastic string were measured experimentally, see the supplemental information (SI) available online at stacks.iop.org/PS/97/035702/mmedia for further details, and found: Young's modulus $E = (4.40 \pm 0.56) \times 10^6$ Pa, Poisson's ratio $\nu = (1.30 \pm 0.31) \times 10^{-2}$, and density $\rho = (9.44 \pm 0.05) \times 10^2$ kg m^{-3}. We also considered the material properties of the metal masses as: Young's modulus $E = 7.00 \times 10^9$ Pa, Poisson's ratio $\nu = 0.340$, and density $\rho = (3.52 \pm 0.17) \times 10^3$ kg m^{-3}, where ρ was measured experimentally, see SI, and E and ν are the values of bronze [14].

2.3. Mathematical methods

A further confirmation of our experimental results was provided by a theoretical model resembling the mechanical SSH model. A schematic representation of our device is shown in figure 2. The equations of motion for the vertical displacement of the pth A site and pth B site, y_p^A and y_p^B, respectively, are derived in terms of the mass m of each site and the intracell (intercell) elasticity constant k_1 (k_2), distance d_1 (d_2), and string elongation Δx_1 (Δx_2) as follows:

$$\begin{aligned} \ddot{y}_p^A + \alpha(y_p^A - y_{p+1}^B) + \beta(y_p^A - y_p^B) = 0, \\ \ddot{y}_p^B + \alpha(y_p^B - y_{p-1}^A) + \beta(y_p^B - y_p^A) = 0. \end{aligned} \tag{1}$$

Here $\alpha = \frac{k_1 \Delta x_1}{m(d_1 + \Delta x_1)}$ and $\beta = \frac{k_2 \Delta x_2}{m(d_2 + \Delta x_2)}$. Assuming discrete translational symmetry, we can apply the Bloch theorem and impose periodic solutions of the form $y_p^A(t) = a_0 e^{-i(\omega t - \kappa \Lambda p)}$ and $y_p^B(t) = b_0 e^{-i(\omega t - \kappa \Lambda p)}$, where ω is the angular frequency, $\Lambda = d_1 + d_2$ is the lattice constant, and $\kappa \in \left[-\frac{\pi}{\Lambda}, \frac{\pi}{\Lambda}\right]$ is the wavenumber. Substituting these imposed solutions into equation (1) yields the matrix equation

$$\begin{pmatrix} \alpha + \beta & -\alpha e^{-i\kappa\Lambda} - \beta \\ -\alpha e^{i\kappa\Lambda} - \beta & \alpha + \beta \end{pmatrix} \begin{pmatrix} y_p^B(\kappa) \\ y_p^A(\kappa) \end{pmatrix} = \omega^2 \begin{pmatrix} y_p^B(\kappa) \\ y_p^A(\kappa) \end{pmatrix}. \tag{2}$$

It is well-known that equation (2) generates the dispersion relation of our system. It is important to notice that the bands had winding numbers of 0 for $d_2/d_1 > 1$ and 1 for $d_2/d_1 < 1$, confirming the topological nature of our system, see SI for further details.

We can rewrite equation (2) for each of our 10 sites as a 10×10 eigenvalue problem [2]:

$$\begin{pmatrix} \alpha+\beta & -\beta & 0 & 0 & 0 & 0 & 0 & 0 & 0 & 0 \\ -\beta & \alpha+\beta & -\alpha & 0 & 0 & 0 & 0 & 0 & 0 & 0 \\ 0 & -\alpha & \alpha+\beta & -\beta & 0 & 0 & 0 & 0 & 0 & 0 \\ 0 & 0 & -\beta & \alpha+\beta & -\alpha & 0 & 0 & 0 & 0 & 0 \\ 0 & 0 & 0 & -\alpha & \alpha+\beta & -\beta & 0 & 0 & 0 & 0 \\ 0 & 0 & 0 & 0 & -\beta & \alpha+\beta & -\alpha & 0 & 0 & 0 \\ 0 & 0 & 0 & 0 & 0 & -\alpha & \alpha+\beta & -\beta & 0 & 0 \\ 0 & 0 & 0 & 0 & 0 & 0 & -\beta & \alpha+\beta & -\alpha & 0 \\ 0 & 0 & 0 & 0 & 0 & 0 & 0 & -\alpha & \alpha+\beta & -\beta \\ 0 & 0 & 0 & 0 & 0 & 0 & 0 & 0 & -\beta & \alpha+\beta \end{pmatrix} \mathbf{y} = \omega^2 \mathbf{y}, \quad \mathbf{y} = \begin{pmatrix} y_1^B \\ y_1^A \\ y_2^B \\ y_2^A \\ y_3^B \\ y_3^A \\ y_4^B \\ y_4^A \\ y_5^B \\ y_5^A \end{pmatrix}. \tag{3}$$

Solving for the eigenvalues of equation (3) gave us angular eigenfrequencies ω^2, which we converted to linear frequencies to compare with the frequencies we observed experimentally.

3. Results

The phase transitions from trivial to metallic to topological phases are shown in figure 3. The experimental (black markers), numerically calculated (red lines), and theoretically calculated (blue markers) frequencies for d_2/d_1 ratios of 3 (trivial II), 2 (trivial I), 1 (metallic), 1/2 (topological I), and 1/3 (topological II) are plotted with

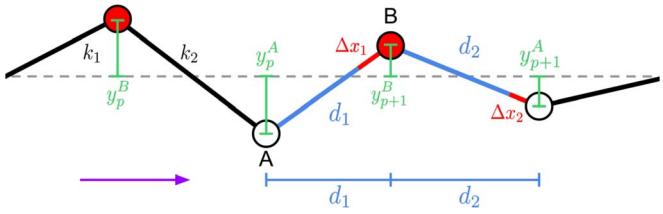

Figure 2. Diagram of a mechanical 1D-SSH model with A and B sites separated by elastic string of intracell (intercell) length d_1 (d_2) and spring constant k_1 (k_2). The purple arrow in the bottom left indicates the direction of wave propagation.

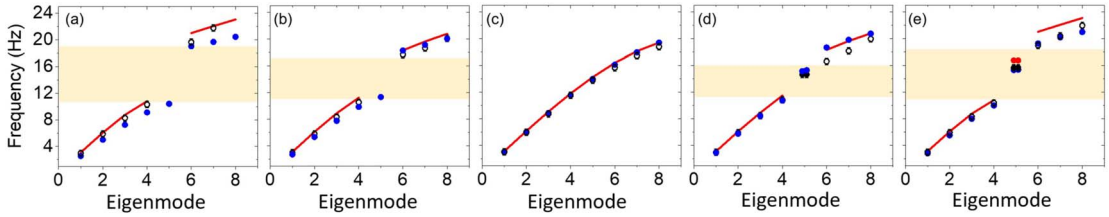

Figure 3. Experimental (black markers), simulated (red lines), and calculated (blue markers) eigenfrequencies of the mechanical 1D-SSH model. From left to right, the configuration is (a) trivial II, (b) trivial I, (c) metallic, (d) topological I, and (e) topological II. The solid black markers represent experimentally observed edge modes. The shaded regions signify the experimentally observed band gaps for the trivial and topological phases in which either no modes or only edge modes were found.

the experimentally observed band gaps shown as shaded yellow regions. It is possible to see that the band gap had a magnitude of 9.2 Hz $\pm$ 0.5 Hz in the trivial II case, figure 3(a), that decreased to 4.5 Hz $\pm$ 0.5 Hz for the trivial I case, figure 3(b), and disappeared for the metallic case, figure 3(c), as expected. A 5.5 Hz $\pm$ 0.5 Hz band gap reopened for the topological I case with the appearance of two edge modes at 14.6 Hz $\pm$ 0.5 Hz, figure 3(d), and widened again to 8.7 Hz $\pm$ 0.5 Hz for the topological II case, with two edge modes at 15.6 Hz $\pm$ 0.5 Hz, figure 3(e). It is important to note that even when there were differences in the band gaps after the topological phase transitions occurred, our measured uncertainty allowed us to conclude that the values were indistinguishable among them.

Our experimental findings confirmed that our mechanical system presented topological transitions with the existence of two edge states inside the band gap. As it is clear from figure 3, the numerically and theoretically calculated frequencies differed from the experimental ones. This was likely a result of damping effects in the experimental system that neither the numerical nor the theoretical models accounted for. Regardless of the specific frequencies of the higher modes, our three approaches showed a clear phase transition between configurations and the existence of edge states in configurations where $d_2/d_1 < 1$.

With the aim of performing a better observation of the shape of the normal modes in the topological II case, figure 4 shows the eigenfrequencies as in figure 3(e) with an image of each experimental and numerically calculated mode on the right side. In order to increase the visibility of the modes, we have doubled the height of each picture while preserving their original width. The modes showed in figure 4 were excited with an amplitude of 0.6 cm $\pm$ 0.1, except for figures 4(g)–(i) that were excited with 0.75 cm $\pm$ 0.1 cm for better observation. The inset below each picture shows the corresponding numerically calculated mode. The insets have the same horizontal scale as the experimental pictures, but the transverse displacements for the numerically calculated modes are on the order of 10^{-2} m. It is clear that the numerical results for the frequencies and shapes of resonant modes matched finely with the experimental ones.

Similarly, figures 4(e) and (f) show the left and right edge states, respectively. It is clear that the edge states were localized to the excited side of the device. In a quantum 1D-SSH system, the energy E of each edge state site N is given by $E = \exp\left(-N \ln\left(\frac{v}{w}\right)\right)$, where v and w are the intracell and intercell electron hopping probabilities, respectively [2]. Our mechanical system clearly showed a trend described by this equation, i.e. there was an exponential decay in the amplitude of oscillation as the wave moved away from the excited site.

In order to confirm our previous statement, we calculated the energy of each A site of the topological II configuration as $E = \frac{1}{2}k_A y^2$, which is shown in figure 5. Here k_A and y are the transverse elasticity constant and the transverse displacement of each A site, respectively. It is clear that our experimental data fit an exponential decay, shown by the red lines in figures 5(a) and (b), that depended on d_2/d_1, as expected. Our mechanical

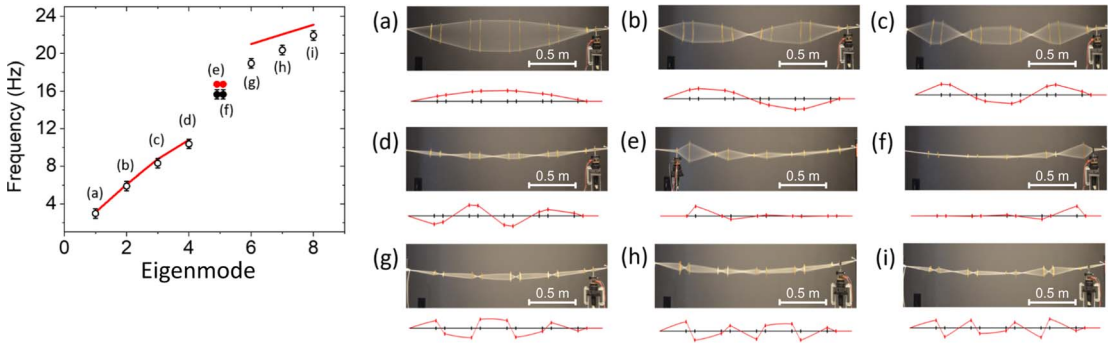

Figure 4. Experimental (black markers) and simulated (red lines) eigenfrequencies of the topological II case, as shown in figure 3(e). The pictures to the right are the (a) first, (b) second, (c) third, (d) fourth, (e) left edge, (f) right edge, (g) sixth, (h) seventh, and (i) eighth modes identified in the mechanical 1D-SSH model. The insets below each picture represent the shape of the simulated modes. All pictures have been doubled in height with respect to figure 1 for better observation.

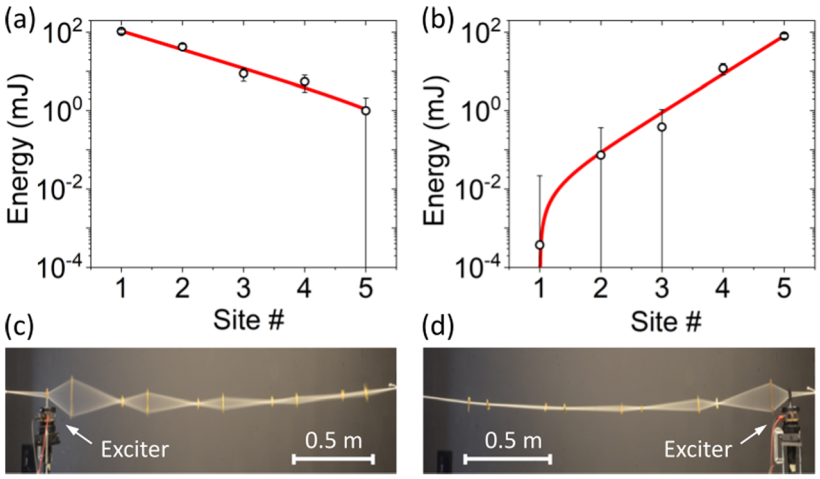

Figure 5. Energy as a function of site number for the (a) left and (b) right edge modes of the topological II case. The red lines represent the numerical fits of the data. Pictures of the experimentally observed (c) left and (d) right edge modes are shown below. The height of the pictures has been doubled with respect to figure 1 for better observation.

system therefore obeys a similar relationship between energy and site number in edge states as is found in quantum 1D-SSH systems [2]. Moreover, we have calculated the critical exponent near the critical point and found that the energy decay constant is proportional to the reciprocal of $v - w$, i.e. $\nu = 1$, as expected in the SSH model [15], see the SI for further details.

Finally, we determined the robustness of the edge modes. We performed numerical simulations shifting the excitation position with respect to the first A site from right to left in figure 1. The excitation position was shifted from −3 cm to 3 cm with 0 cm the position of the B site. As showed before, an edge state should show a exponentially decay on its potential energy, see figure 5. We found that the potential energy decays exponentially, no matter the position of the excitation, see SI.

4. Conclusion

In conclusion, we have demonstrated phase transitions in a one-dimensional mechanical topological insulator based on the SSH model. Experimental evidence, supported by numerical and theoretical models, showed that our system presented a trivial band gap that becomes a topological one by continuous deformation of the crystal lattice. The existence of the two edge states, corresponding to each edge of the system, allowed us to determine the topological nature of the device. In addition, we have proved the exponential decay of the energy of each site when the edge states were excited, as predicted by a quantum 1D-SSH model. We believe that all the presented evidence is enough to conclude that the observed phenomena were in fact the topological phase transitions of our device. The simplicity and easily accessible materials used in our device allows for the construction and

observation of topological transitions in a very simple classical system that can be implemented in any research and teaching lab.

Acknowledgments

Juan M Merlo acknowledges Vassar College for startup funding number ST000057 and the URSI program support.

Data availability statement

The data that support the findings of this study are available upon reasonable request from the authors.

Authors' contributions

JMM conceived the project; LT and JMM performed the experiments and wrote the manuscript; all authors contributed to the discussion and interpretation of the results.

Author declarations

Conflict of interest

The authors have no conflicts to disclose.

ORCID iDs

Luke Thatcher https://orcid.org/0000-0001-9986-5896
Juan M Merlo https://orcid.org/0000-0002-3956-0940

References

[1] Hasan M Z and Kane C L 2010 Colloquium: topological insulators *Rev. Mod. Phys.* **82** 3045–67
[2] Asbóth J K, Oroszlány L and Pályi A 2016 A short course on topological insulators *Lecture Notes in Physics* vol 919 (Berlin: Springer)
[3] Hämäläinen S K, Sun Z, Boneschanscher M P, Uppstu A, Ijäs M, Harju A, Vanmaekelbergh D and Liljeroth P 2011 Quantum-confined electronic states in atomically well-defined graphene nanostructures *Phys. Rev. Lett.* **107** 236803
[4] Chaplain G J, De Ponti J M, Aguzzi G, Colombi A and Craster R V 2020 Topological rainbow trapping for elastic energy harvesting in graded su-schrieffer-heeger systems *Phys. Rev. Applied* **14** 054035
[5] Chen Z-G, Wang L, Zhang G and Ma G 2020 Chiral symmetry breaking of tight-binding models in coupled acoustic-cavity systems *Phys. Rev. Applied* **14** 024023
[6] Li X, Meng Y, Wu X, Yan S, Huang Y, Wang S and Wen W 2018 Su-schrieffer-heeger model inspired acoustic interface states and edge states *Appl. Phys. Lett.* **113** 203501
[7] Merlo J M, Wu X, Kempa K and Naughton M J 2021 All-optical logic gates based on anomalous floquet photonic topological insulator structures *J. Opt.* **23** 065001
[8] Wu X, Ye F, Merlo J M, Naughton M J and Kempa K 2018 Topologically protected photonic edge states in the visible in plasmo-gyroelectric metamaterials *Adv. Opt. Mater.* **6** 1800119
[9] Pal R K and Ruzzene M 2017 Edge waves in plates with resonators: an elastic analogue of the quantum valley hall effect *New J. Phys.* **19** 025001
[10] Bösch C, Dubček T, Schindler F, Fichtner A and Serra-Garcia M 2020 Discovery of topological metamaterials by symmetry relaxation and smooth topological indicators *Phys. Rev.* B **102** 241404
[11] Su W P, Schrieffer J R and Heeger A J 1979 Solitons in polyacetylene *Phys. Rev. Lett.* **42** 1698–701
[12] Yin J, Ruzzene M, Wen J, Yu D, Cai L and Yue L 2018 Band transition and topological interface modes in 1d elastic phononic crystals *Sci. Rep.* **8** 6806
[13] Gómez B J, Repetto C E, Stia C R and Welti R 2007 Oscillations of a string with concentrated masses *Eur. J. Phys.* **28** 961–75
[14] AZoMaterials, Copper alloys—bronzes, (2021) (https://azom.com/properties.aspx?ArticleID=62)
[15] Chen W, Legner M, Ruegg A and Sigrist M 2017 Correlation length, universality classes, and scaling laws associated with topological phase transitions *Phys. Rev.* B **95** 075116